JOURNAL OF SOLID STATE CHEMISTRY 47, 151–163 (1983)

The Hollandite-Related Structure of $Ba_2Ti_9O_{20}$

G. GRZINIC AND L. A. BURSILL*

School of Physics, University of Melbourne, Parkville, 3052, Victoria, Australia

AND DAVID J. SMITH

High Resolution Electron Microscope, University of Cambridge, Free School Lane, Cambridge CB2 3RQ, England

Received November 22, 1982

The crystal structure of $Ba_2Ti_9O_{20}$ has been determined by comparison of experimental high-resolution electron micrographs with images simulated using structural models deduced from the micrographs in conjunction with crystallochemical principles. The structure consists of lamellae of hollandite-type structure alternating with $BaTiO_3$-like units, which effectively immobilize the Ba ions. This material should be relatively more leach resistant to attack by aqueous sodium chloride solutions. The structure determination clarifies the observation that this material has unique properties as a microwave resonator, compared with other barium and alkali titanate structures.

Introduction

The structures of the hollandite-related phases $Ba_xGa_{2x}Ti_{8-2x}O_{16}(0.80 \leq x \leq 1.33)$ and $Ba_xMg_xTi_{8-x}O_{16}(0.80 \leq x \leq 1.33)$ were analyzed by high-resolution electron microscopy (HREM) and diffraction (*1*). Three basic ordered structures were found, for $x = 0.80$, 1.20 and 1.33, with intermediate stoichiometries which could be described in terms of short-range-ordered domain structures, containing mixed intergrowths. An independent study using X-ray diffraction confirmed the structure of $x = 1.33$ (*2*) for $Ba_xAl_{2x}Ti_{8-2x}$, and it was also reported that hollandite extends to $x \sim 0.3$. Bursill and Grzinic (*1*) found, however, that new superlattice phases, related to hollandite, but readily distinguishable from it using electron diffraction techniques, occurred for $x < 0.8$. "Hollandites" having $x < 0.80$ are relatively very stable, strongly resisting attack by aqueous sodium chloride solutions (*3*). In view of the potential application of this phase for the immobilization of radioactive Cs^{137} in high-level nuclear wastes (*3*), further HREM studies were made of the intricate domain structures and intergrowth phases which appear for preparations having $x < 0.80$. It transpired that these were often structurally related to $Ba_2Ti_9O_{20}$ (*4*), whose structure had not yet been described. Consideration of the HREM images has since led us to a structural model for $Ba_2Ti_9O_{20}$ which yields good computer-simulated image matches for ax-

*To whom correspondence should be addressed.

0022-4596/83 $3.00

ial projections of a triclinic cell a = 14.358 Å, b = 14.095 Å, c = 7.477 Å, α = 95.53°, β = 100.55°, and γ = 89.95°.

The structural relationship of this phase to that of hollandite then readily leads to an explanation of the complex fine-scale intergrowth textures found for $Ba_xAl_{2x}Ti_{8-2x}O_{16}$ ($x < 0.80$) and $Ba_xMg_xTi_{8-x}O_{16}$ ($x = 0.67$) preparations. The intergrowth principles and defect structures are discussed briefly below but detailed enumeration and interpretation is left for later publications (*5*).

Consideration of the structure of $Ba_2Ti_9O_{20}$ immediately suggests why "hollandite" preparations having $x \sim 0.2$–0.3 should have increased leach resistance. It also gives a microscopic explanation for the unique dielectric properties exhibited by $Ba_2Ti_9O_{20}$ which make it useful as a microwave resonator.

Experimental

A sample of stoichiometric $BaTi_5O_{11}$ was prepared by mixing weighed $BaCO_3$ and TiO_2 powders (Koch–Light, 4N) and pressing pellets, which were heated in sealed platinum tubes at a temperature of 1350°C for 14 days. As reported (*6*) special care is required to obtain single phase $Ba_2Ti_9O_{20}$, which decomposes in a peritectoidal reaction at 1420°C. The phase analysis of O'Bryan and Thompson (*6*) and more recent work (*4, 7*) show that $Ba_{2+x}Ti_9O_{20+x}$ is essentially stoichiometric ($x < 0.02$) and that it coexists with TiO_2 for $BaTi_5O_{11}$ preparations given the above heat treatment. The phases $BaTi_5O_{11}$ and $BaTi_6O_{13}$ (*8, 9*) do not occur as stable phases at subsolidus temperatures, but most likely result for specimens quenched from above the solidus. Neither of these phases appeared in our preparations.

Fragments of the pellets were ground under chloroform, in an agate mortar with pestle, and deposited onto carbon lace support film. The thin edges were examined using a high-tilt side-entry goniometer to allow diffraction data to be collected from several principal axes. Some specimens were then examined using a homemade goniometer (*10*) in a JEOL-100C electron microscope having electron optical parameters: spherical aberration coefficient C_s = 0.7 mm, chromatic aberration coefficient C_c = 1.05 mm, and focal length f_0 = 1.35 mm. Crystals were tilted into the [101], [100], [010], and [001] projections and images recorded at magnifications of 330,000× to 1,000,000× using objective lens defocus values -200 Å $\geq \Delta f \geq -1500$ Å and focused illumination (0.8–1.2 mrad). The so-called "structure images" (*11*) should be obtained for $\Delta f = -600$ Å at 2.9 Å resolution, provided the crystals are sufficiently thin.

The solution of the structure was greatly assisted by obtaining a [010] projection at increased resolution using the Cambridge University HREM; with accelerating potential 500 kV, C_s = 3.5 mm, and defocus range -1500 Å $\leq \Delta f \leq -100$ Å. In this case the structural resolution is approximately 2.0 Å (*12*).

Results

1. Electron Diffraction Analysis of $Ba_2Ti_9O_{20}$

Figure 1a–c shows [100], [010], and [001] reciprocal-lattice sections. The patterns were indexed using triclinic cell parameters derived from the tetragonal cell parameters of hollandite by noting the relationship of the structure to the corresponding projections of hollandite, i.e.,

$$[100] \cong \| [001]_h$$
$$[010] \cong \| [110]_h$$
$$[001] \cong \| [111]_h.$$

Accurate cell parameters became available from X-ray diffraction studies during the writing of this paper (see Ref. (*13*)), and

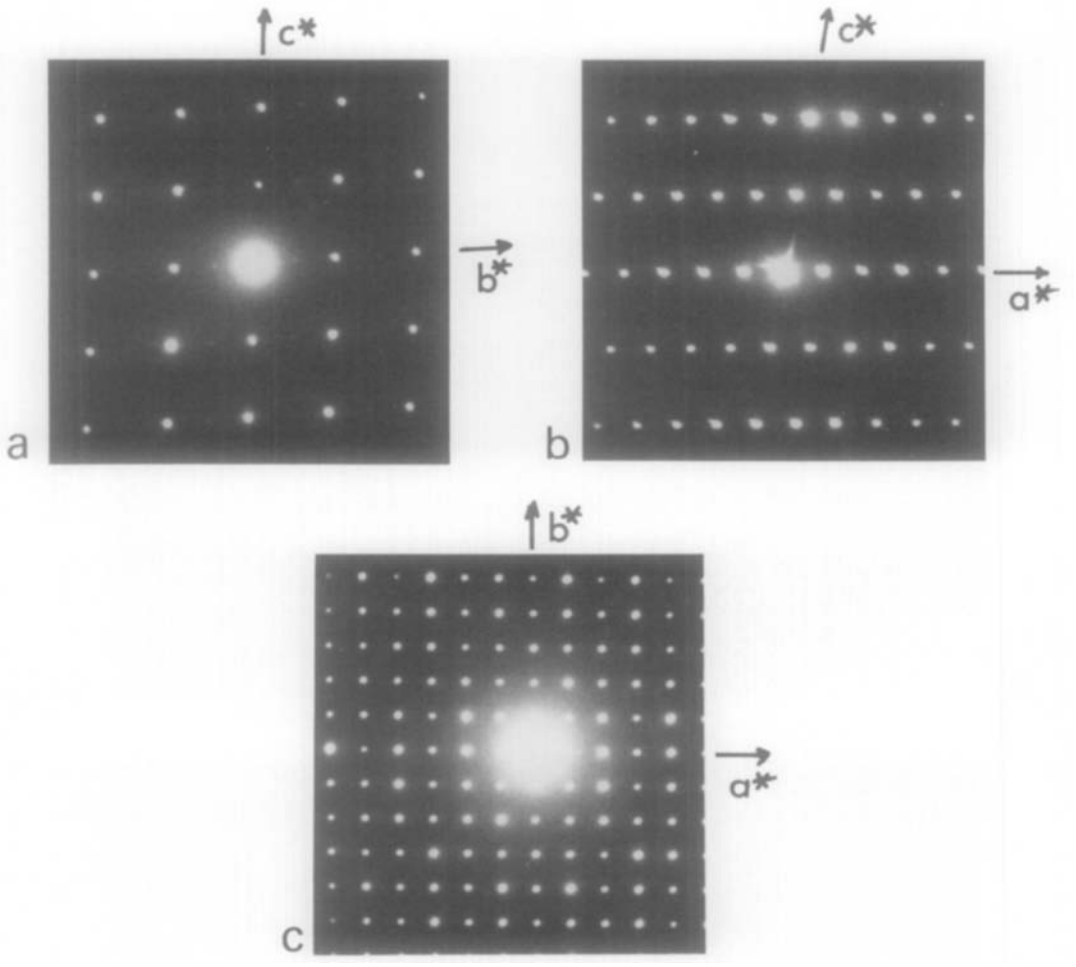

FIG. 1. Diffraction patterns of $Ba_2Ti_9O_{20}$ for (a) [100], (b) [010], and (c) [001] axial projections.

these are used here for the computer simulations and discussion.

2. *HREM Images of $Ba_2Ti_9O_{20}$*

Figure 2a,b gives [100] and [001] projections, obtained at 100 kV, whereas Fig. 3a,b shows [010] projections obtained at 100 and 500 kV, respectively. Figure 4a gives an example of an intergrowth defect (a slab of 21 $\times$ 14 Å^2 structure within the 14 $\times$ 14 Å^2 $Ba_2Ti_9O_{20}$) imaged at 100 kV and viewed along [001], whereas Fig. 4b shows an extensive array of the 21 $\times$ 14 Å^2 structure, imaged at 500 kV. In this case the specimen stoichiometry was $Ba_{0.8}Al_{1.6}Ti_{6.4}O_{16}$ which had been heated at 1350°C for 5 days. This is included here since the increased resolution was significant in enabling some details of the structure of $Ba_2Ti_9O_{20}$ to be determined. In general very much more complex textures occurred in $Ba_xAl_{2x}Ti_{8-2x}O_{16}$ ($x \leq 0.8$) and $Ba_xMg_xTi_{8-x}O_{16}$ ($x = 0.67$) preparations (*5*) with intergrowths having dimensions 14 $\times$ 21 Å^2, 14 $\times$ 6 Å^2, 7 $\times$ 6 Å^2, and 7 $\times$ 14 Å^2 in addition to the 14 $\times$ 14 Å^2 structure of $Ba_2Ti_9O_{20}$. Examples of the image contrast were given in a preliminary report

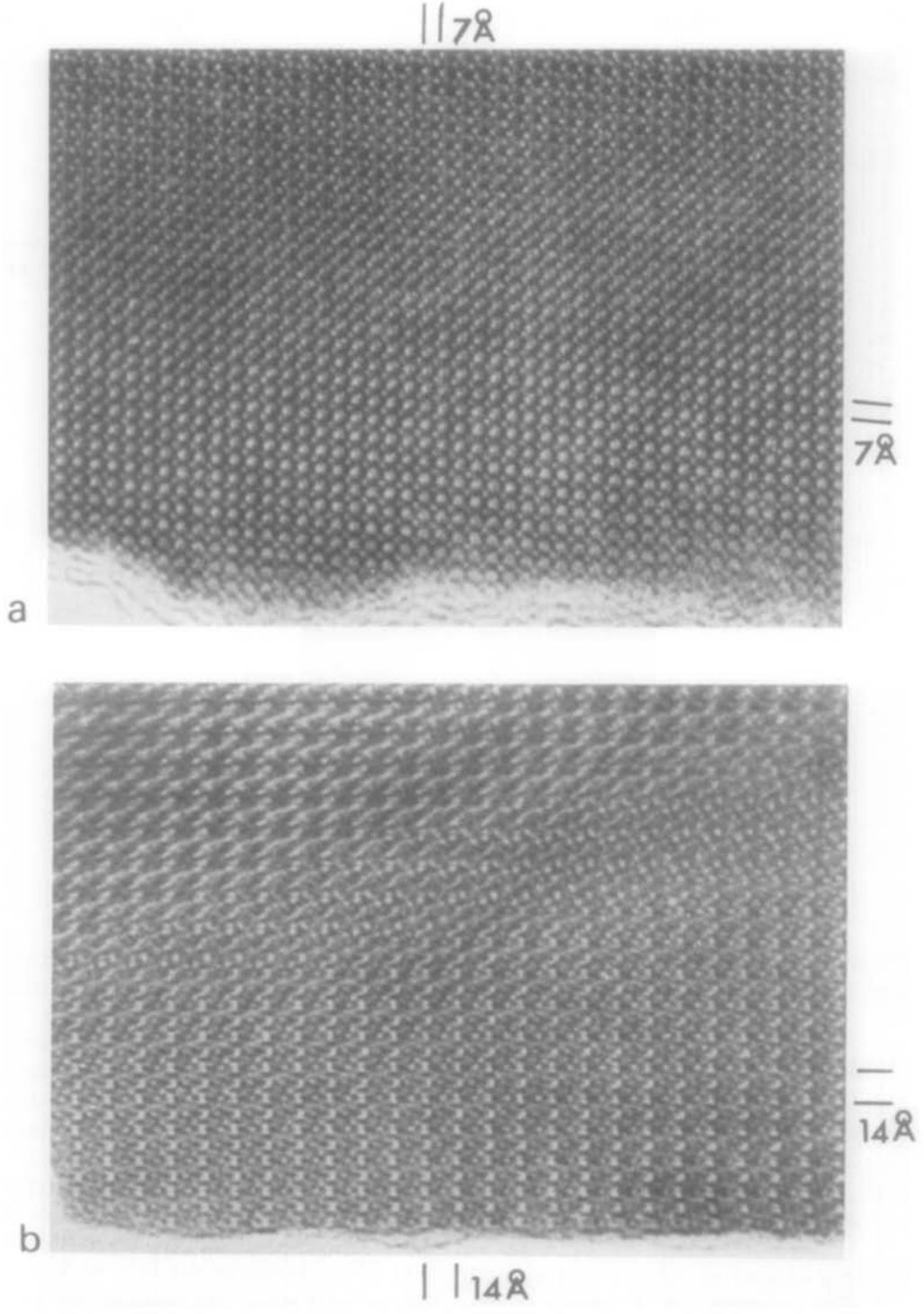

FIG. 2. HREM 100 kV images of $Ba_7Ti_9O_{20}$ for (a) [100] and (b) [001] axes; approximate resolution is 3 Å.

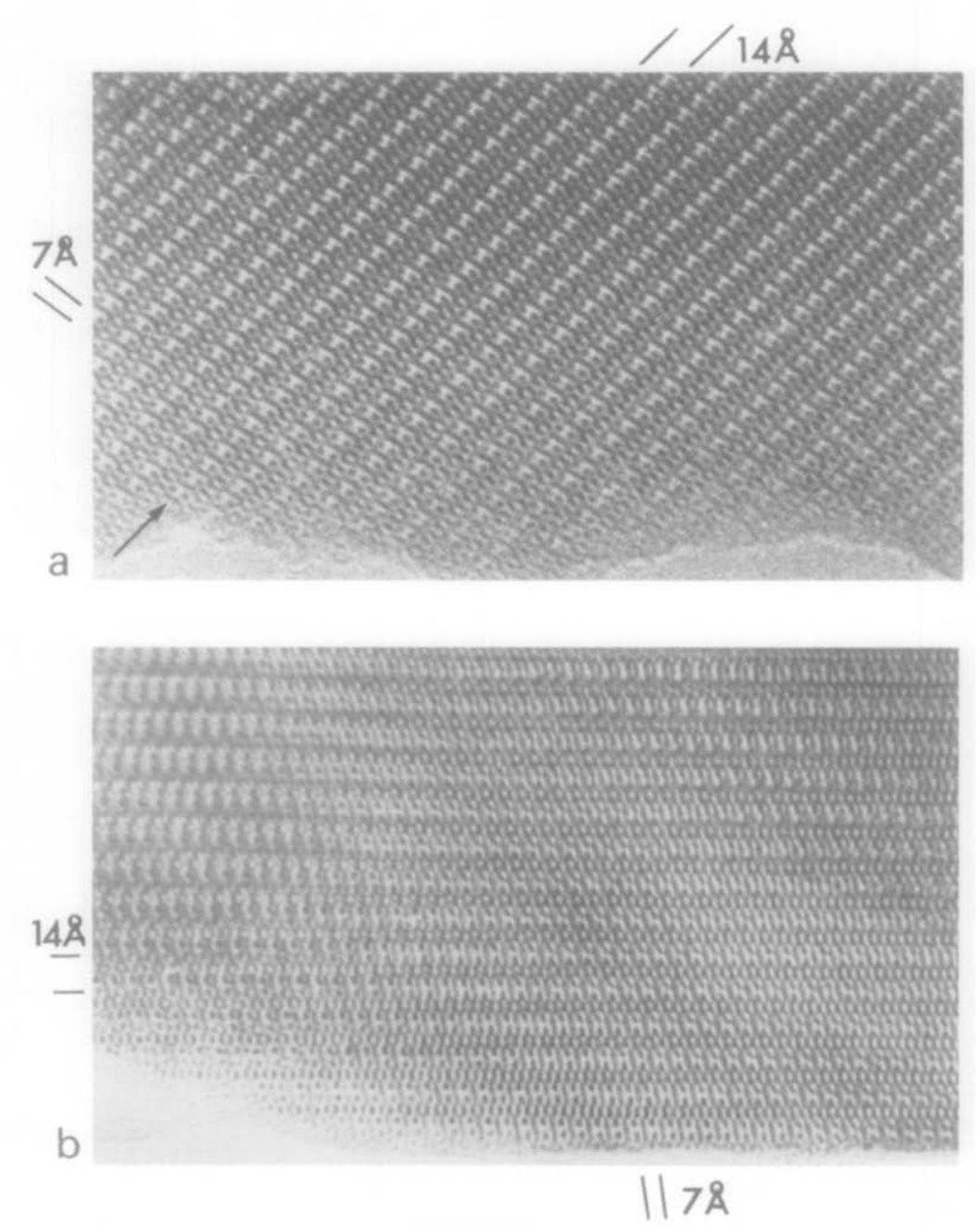

FIG. 3. HREM images of $Ba_2Ti_9O_{20}$ for [010] projection at (a) 100 kV and (b) 500 kV.

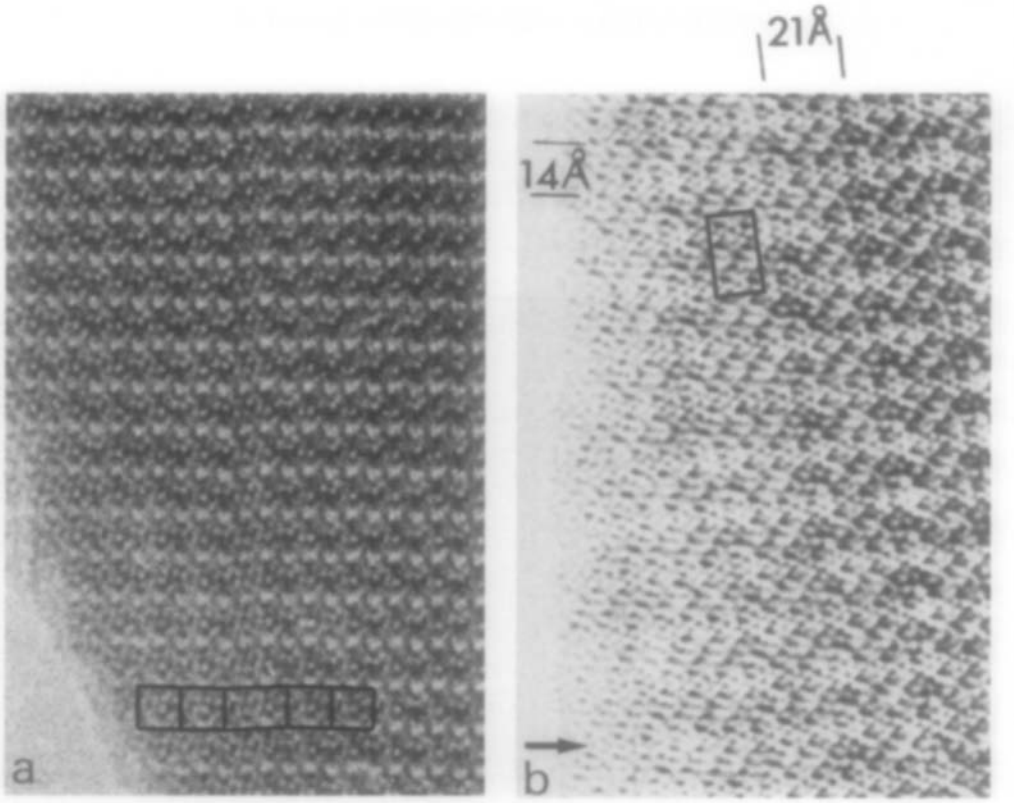
21Å
14Å
a
b

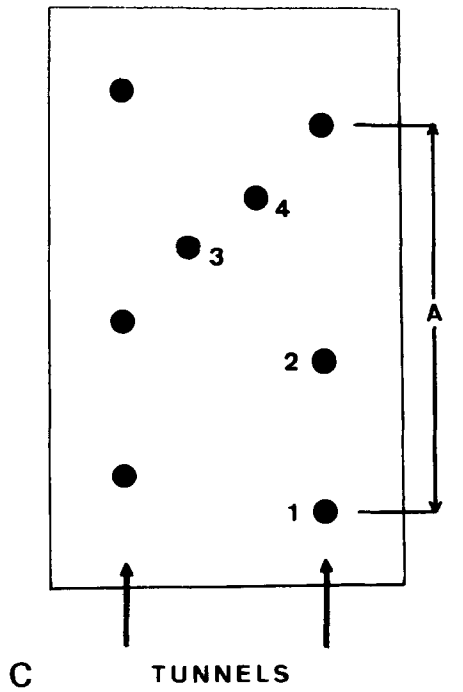
4
3
2
1
A
C
TUNNELS

(*14*). Figure 5 shows a 500 kV image for the [101] projection.

Derivation of the Structure of $Ba_2Ti_9O_{20}$

The [100] diffraction pattern (Fig. 1a) and corresponding image (Fig. 2a) suggest a close relationship to the $[100]_h$ projection of hollandite (cf. Fig. 3 of ref. (*1*) and Fig. 7 of ref. (*15*), respectively). There is a lowering of projection symmetry from *4mm* to *2mm* plus a doubling along [010], indicated by faint superlattice spots in Fig. 1a. The interaxial angle is significantly changed from 90 to 95°. The [010] image (Fig. 3a,b), which corresponds roughly to the $[110]_h$ projection of hollandite, should therefore display the contents of the "hollandite" tunnels. Note the appearance of (001) slabs containing pairs of dark blobs of intensity within an H-shaped region having bright intensity (arrowed in Fig. 3a), alternating with narrower strips of bright–dark intensity having approximately 3.6 Å periodicity along k_{100}. The wider slabs show very similar contrast features to computer simulations of the $[110]_h$ projection, with the dark spots indicating the presence of Ba^{2+} ions in the tunnels. The lines of dark intensity correspond to the double-edge-shared strips of $[TiO_6]$ octahedra which form the MX_2 framework structure of hollandite (Figs. 6b and 7). The 500 kV image for the [001] projection of the 21 × 14 $Å^2$ intergrowth structure (Fig. 4b) also indicated hollandite-type slabs. Thus the slabs showing a regular array of black and white spots, arrowed in Fig. 4b, closely resemble computer-calculated images of $[111]_h$ of hollandite. The corresponding 100 kV images (Fig. 4a) had insufficient resolution to make this relationship to hollandite clear. The latter proved very sensitive to objective lens defocus, specimen thickness, and slight tilts of the crystal or incident beam off the optic axis of the objective lens. The so-called "structure image" was relatively easy to locate at 500 kV. Thus many of the earlier 100 kV images gave misleading suggestions about the relative offset of adjacent hollandite-type slabs. Close examination of thin areas of the 500 kV image (Fig. 4b) shows dark spots which represent Ba^{2+} positions, by comparison with $[111]_h$ computer simulations. Figure 4c shows an enlarged representation of the Ba atom positions inside the rectangle indicated on Fig. 4b. Black spots labeled 1 and 2 represent Ba^{2+} located at normal tunnel sites of hollandite. Initially it was assumed that spots 3 and 4 represent Ba positions since they are of similar strength to spots 1 and 2. This locates Ba 3 and 4 inside the octahedral framework separating the tunnels; specifically at distances of $\frac{1}{3}$ and $\frac{2}{3}$ along a line joining the centers of two adjacent tunnels, which suggests that Ba replaces oxygen in the framework. Reference to the [010] images then located Ba^{2+} as shown in Fig. 6a. Further structural considerations, taking into account charge-balance requirements and the diffraction patterns, lead to the complete structural model shown in Fig. 8a–c. This figure gives the structure viewed along [001], where three distinct levels of octahedra occur along the 7.5 Å projection axis. There are four formula units per unit cell, with four Ba atoms at normal "hollandite" tunnel sites and the remaining four substituting for oxygens in the framework as shown. Fig. 6a,b gives a

FIG. 4. (a) 100 kV HREM image of $Ba_2Ti_9O_{20}$ for [001] projection showing a 14 × 21 Å lamellar intergrown within basic 14 × 14 Å structure. (b) 500 kV HREM image of $Ba_{0.8}Al_{1.6}Ti_{6.4}O_{16}$ preparation showing an extensive array of 14 Å × 21 Å type structure. (c) Schematic enlargement corresponding to Fib. 4b, showing Ba positions within "hollandite tunnels" (1,2) and replacing oxygen in framework (3,4).

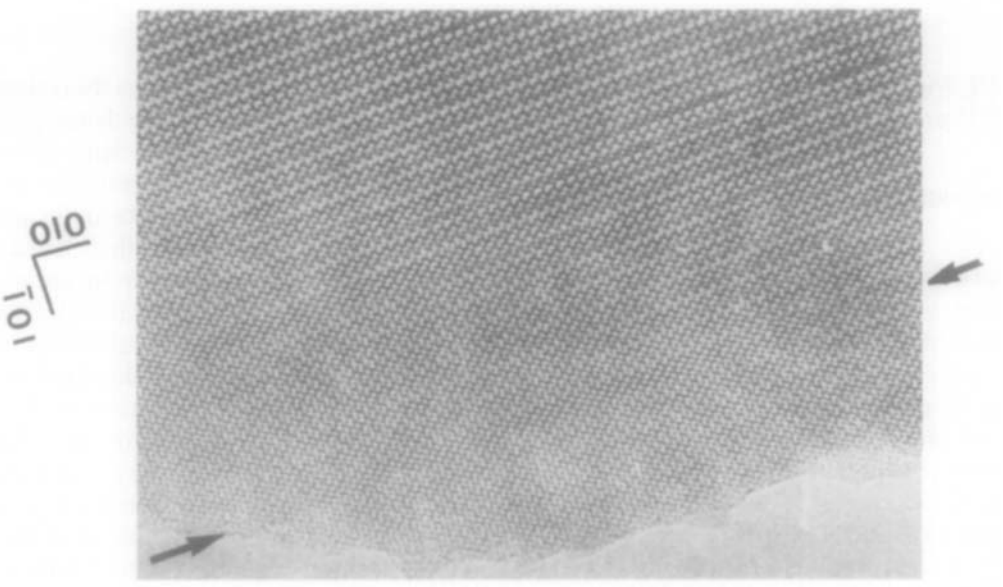

FIG. 5. 500 kV HREM image of $Ba_2Ti_9O_{20}$ in [101] projection. A 14 × 21 Å intergrowth defect is arrowed.

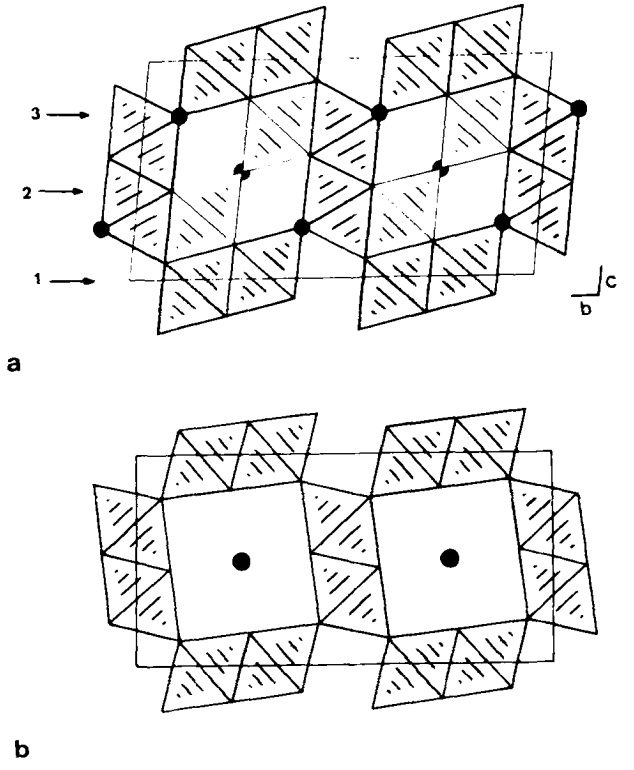

FIG. 6. Structure of $Ba_2Ti_9O_{20}$ (a) viewed along [100]. Black circles show Ba positions. Note (i) distortion of framework compared to hollandite $[001]_h$ projection (b), to give essentially close-packed array with stacking sequence ABCBCA; (ii) Ba sites replacing oxygen in framework; and (iii) $[TiO_6]$ octahedra blocking "hollandite" tunnels.

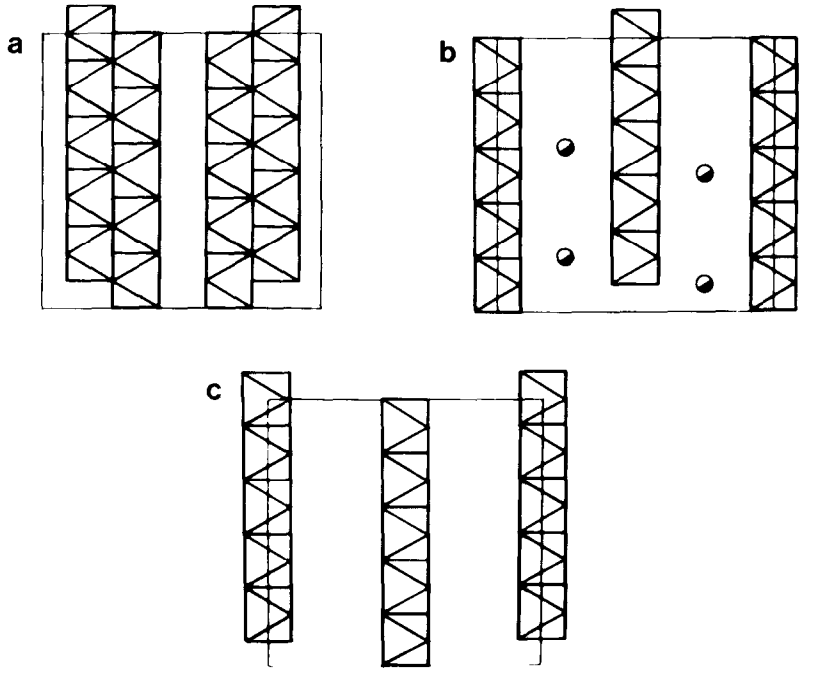

FIG. 7. Arrangement of $[TiO_6]$ octahedra for hollandite structure, viewed approximately along $[111]_h$. Three levels (a–c) superimpose to give 7.5 Å repeat along projection axis.

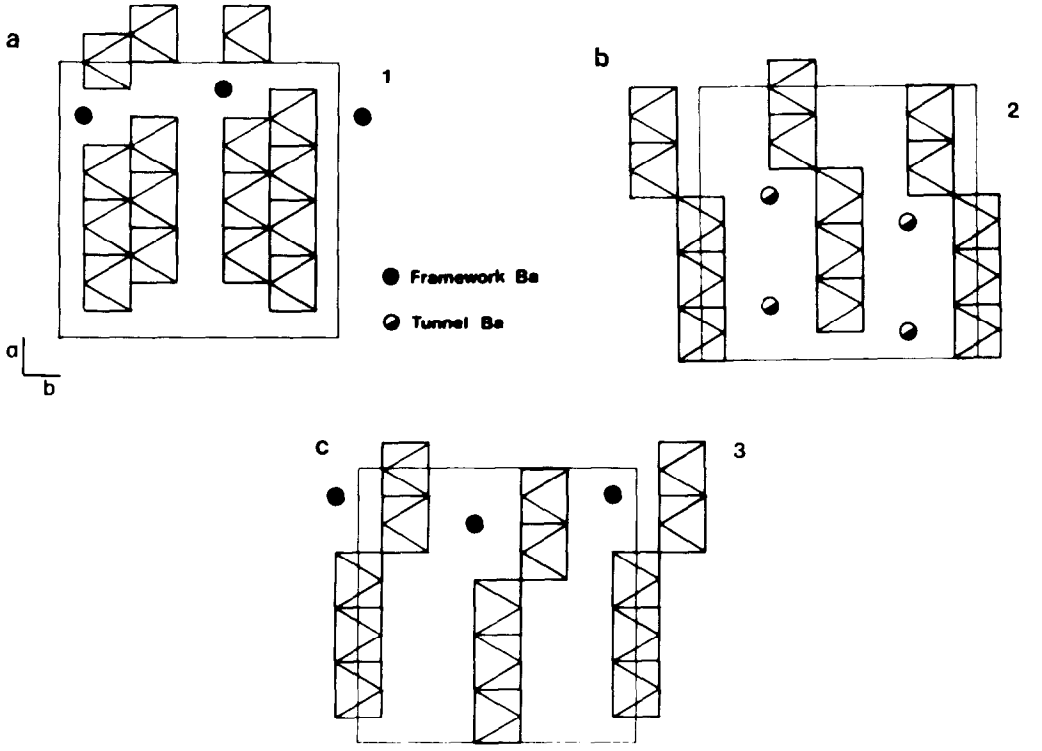

FIG. 8. Arrangement of Ba and $[TiO_6]$ octahedra at three levels (a–c) of unit cell of $Ba_2Ti_9O_{20}$ for [001] (=7.5 Å) projection. Levels (a–c) correspond to sections labeled 1, 2, and 3 in Fig. 6(a).

comparison of the hollandite $[001]_h$ and $Ba_2Ti_9O_{20}$ [100] projections. The octahedral framework is skewed over (sheared) to produce essentially a close-packed array of Ba and oxygen atoms having a mixed stacking sequence ABCBCA. Two of the three Ti atoms originally surrounding the Ba-replaced anion site are displaced into adjacent octahedrally coordinated sites in the "tunnels," generated by the displaced oxygens plus additional oxygens required to charge balance Ba^{2+}. The "shearing" of the framework structure to produce an essentially close-packed Ba + O array provides the mechanism for the change in interaxial angles for the $[100] \equiv [001]_h$ projection. The framework Ba^{+2} have 12-fold coordination. The sequence of sites along the "tunnels" is

O–Ba–vacancy–Ba–O

giving a $5\times[001]_h$ (=14.4 Å) repeat. The electrostatic environment of all Ba^{2+} and Ti^{4+} ions is reasonable, giving electrostatic valence −2 for the oxygens. The $[TiO_6]$ octahedral arrangement around Ba has six of the eight octahedra identically placed as does Ba in the perovskite-type structure of $BaTiO_3$, with the remaining oxygens only slightly displaced from cubooctahedral coordination. In this respect the structure may be regarded as an ordered intergrowth of $BaTiO_3$-like slabs within the hollandite-like slabs. Note that $[TiO_6]$ octahedra join by sharing edges and corners (Fig. 8a–c).

TABLE I

ATOMIC COORDINATES FOR $Ba_2Ti_9O_{20}$

				Barium				
.600	.250	.500	.200	.250	.500	.775	.083	.243
.100	.750	.500	.500	.750	.500	.875	.583	.243
.825	.417	.757	.925	.917	.757			
				Titanium				
.417	.000	.670	.617	.000	.670	.117	.500	.670
.217	.000	.670	.283	.000	.330	.483	.000	.330
.679	.833	.292	.083	.000	.330	.354	.167	.042
.554	.167	.042	.046	.333	.958	.957	.167	.042
.154	.167	.042	.446	.333	.958	.646	.333	.958
.921	.667	.709	.246	.333	.958	.021	.167	.709
.979	.333	.292	.779	.333	.292	.879	.833	.292
.317	.500	.670	.517	.500	.670	.721	.667	.709
.383	.500	.330	.583	.500	.330	.183	.500	.330
.254	.667	.042	.454	.667	.042	.654	.667	.042
.054	.667	.042	.346	.833	.958	.546	.833	.958
.746	.833	.958	.146	.833	.958	.821	.167	.709
				Oxygen				
.441	.083	.910	.641	.083	.910	.841	.083	.910
.041	.083	.910	.241	.083	.910	.334	.250	.833
.534	.250	.833	.734	.250	.833	.934	.250	.833
.134	.250	.833	.425	.417	.757	.625	.417	.757
.193	.917	.424	.225	.417	.757	.375	.083	.243
.575	.083	.243	.900	.750	.500	.975	.083	.243
.175	.083	.243	.266	.250	.167	.466	.250	.167
.666	.250	.167	.866	.250	.167	.066	.250	.167
.359	.417	.090	.559	.417	.090	.759	.417	.090
.959	.417	.090	.159	.417	.090	.307	.083	.577
.507	.083	.577	.707	.083	.577	.907	.083	.577
.107	.083	.577	.293	.417	.424	.493	.417	.424
.693	.417	.424	.893	.427	.424	.093	.417	.424
.800	.250	.500	.000	.250	.500	.700	.750	.500
.341	.583	.910	.541	.583	.910	.741	.583	.910
.941	.583	.910	.141	.583	.910	.434	.750	.833
.634	.750	.833	.834	.750	.833	.034	.750	.833
.234	.750	.833	.325	.917	.757	.525	.917	.757
.725	.917	.757	.025	.417	.757	.125	.917	.757
.275	.583	.243	.475	.583	.243	.675	.583	.243
.075	.583	.243	.366	.750	.167	.566	.750	.167
.766	.750	.167	.966	.750	.167	.166	.750	.167
.259	.917	.090	.459	.917	.090	.659	.917	.090
.859	.917	.090	.059	.917	.090	.407	.583	.577
.607	.583	.577	.807	.583	.577	.007	.583	.577
.207	.583	.577	.393	.917	.424	.593	.917	.424
.793	.917	.424	.993	.917	.424			

Computer Simulation and Image Matching

For simplicity in deriving the atomic coordinates we assumed a regular close-packed array of (Ba+O) with mixed stacking sequence ABCBCA. Thus Ti and Ba have regular coordinations, and there is one vacant anion site per tunnel. The list of atomic coordinates is given in Table I. This ideal packing gives unit-cell parameters indicated in Table II. The corresponding cell parameters, assuming an unchanged hollandite framework, are also listed. Comparison of these two sets with the observed cell parameters suggests that the framework in fact lies between these two, but closer to close packing than to hollandite. The HREM images are not sensitive to small changes in the precise values of cell parameters, or to small displacements of the ions from their "ideal" sites.

HREM images were simulated using

TABLE II

CELL PARAMETER VARIATIONS FOR "HOLLANDITE" FRAMEWORKS

Cell parameter	Structure		
	Hollandite	$Ba_2Ti_9O_{20}$	Ideal close packing
a	14.36 Å	14.358 Å	14.36 Å
b	14.4 Å	14.095 Å	13.98 Å
c	7.33 Å	7.477 Å	7.55 Å
α	90.0°	95.53°	96.7°
β	100.5°	100.55°	100.5°
γ	90.0°	89.95°	90.0°

standard techniques (*16*); the image matches obtained, after determining specimen thickness and defocus values, are given in Fig. 10a–d for [010] (100 and 500 kV), [001] (100 kV), and [$\bar{1}$01] (500 kV) images.

Details of the electron optical parameters used in image matching are given in the figure captions. The good agreement achieved, especially for the 500 kV images, confirms that the structural model is a reasonable one. The 100 kV images are more sensitive to specimen orientation, incident beam alignment, precise values of crystal thickness and defocus and are clearly affected by incident-beam divergence and chromatic aberration. Thus the degree of image matching obtained here is also reasonable. The present structural determination has been confirmed by a recent X-ray diffraction study (*13*), and further refinement of the structure is best done using that technique.

Discussion

1. Intergrowth and Defect Structures Related to $Ba_2Ti_9O_{20}$

The 21 × 14 Å^2 intergrowth defect requires a repeat of three "tunnels," com-

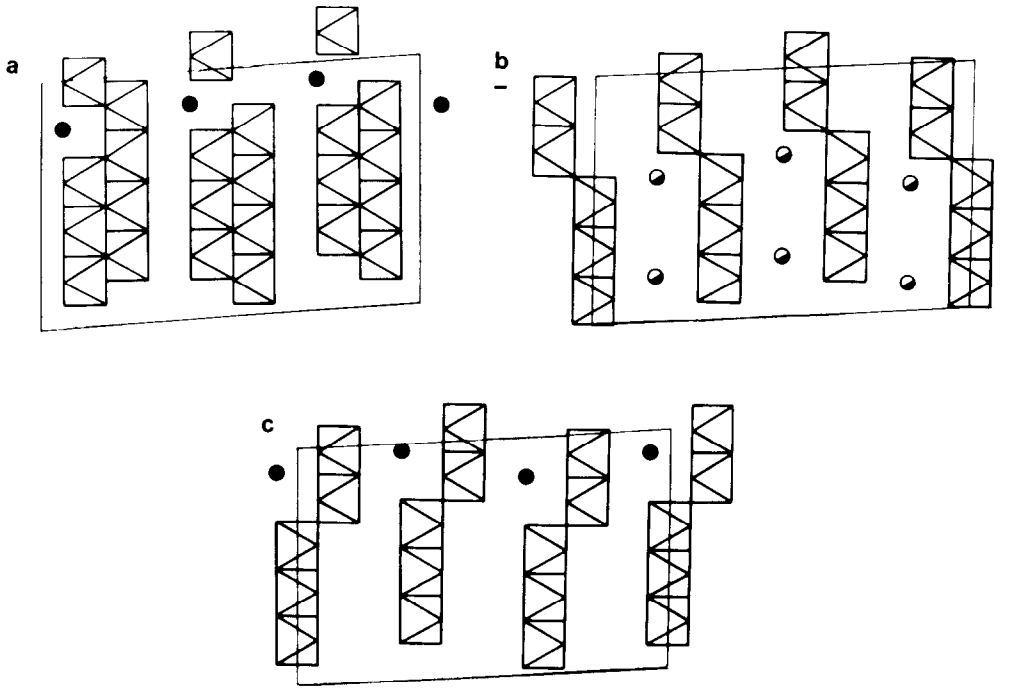

FIG. 9. Corresponding levels (a–c) for the 14 × 21 Å polytypic variation of $Ba_2Ti_9O_{20}$ (cf. Fig. 4a,b).

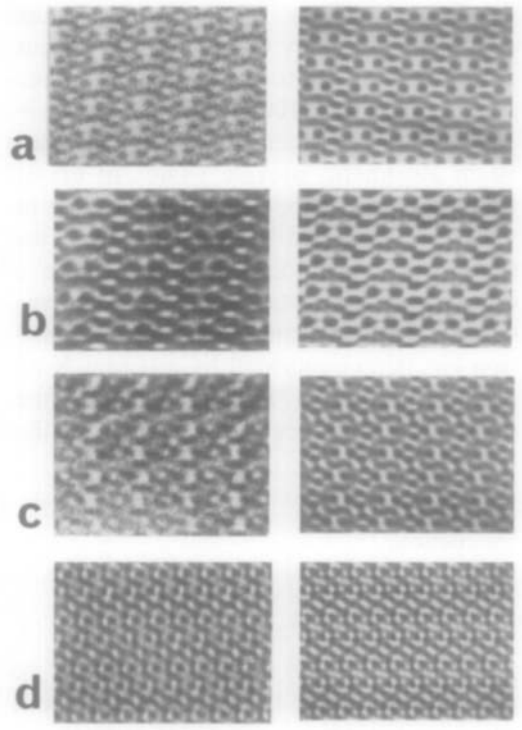

FIG. 10. Computer simulated image matches for (a) 100 kV image along [010] for $\Delta f = -600$ Å, $H = 60$ Å, Resolution (R) = 3 Å, crystal tilt (T) = 0.6 mrad, chromatic effects included; (b) 500 kV image along [010] for $\Delta f = -850$ Å, $H = 90$ Å, $R = 2$ Å, $T = 0.3$ mrad; (c) 100 kV image along [001] for $\Delta f = -550$ Å, $H = 60$ Å, and $R = 3$ Å; (d) 500 kV image along [101] for $\Delta f = -750$ Å, $H = 60$ Å, $R = 2$ Å.

pared with two along [010] for $Ba_2Ti_9O_{20}$. Assuming there is no change in the anion net stacking sequence, we arrive at a triclinic cell for this structure with $a = 14.36$ Å, $b = 21.14$ Å, $c = 7.45$ Å, $\alpha = 95.53°$, $\beta = 100.55°$, and $\gamma = 86.1°$. A model for the Ba occupancies was derived using the HREM images and its structural relationship to $Ba_2Ti_9O_{20}$. The three levels of the structure are given in Fig. 9a–c for the [001] projection. This model has stoichiometry $Ba_2Ti_9O_{20}$ and represents a polytypic variation. Small areas exhibiting a four-tunnel repeat have also been observed in $BaTi_5O_{11}$ preparations. In view of the frequent occurrence of these structures, together with other variations on the basic 14 × 14 Å cell, in preparations containing Al^{3+} or Mg^{2+}, it is possible the polytypic forms may be stabilized by altervalent ions. In an earlier review of titanate structures related to hollandite (*17*) it was shown that Ga^{3+} (and possibly Al^{3+}) could occupy tetrahedral sites within "tunnels", giving elements of the β-Ga_2O_3 type structure. Close inspection of HREM images obtained so far indicates small, but significant differences in the image intensity for specimens giving 21 × 14 $Å^2$ structures, but prepared with and without Al^{3+}. Clearly it is not possible to simply replace Ti^{4+} ions by Al^{3+} ions in the same octahedral sites as are occupied in $Ba_2Ti_9O_{20}$. A charge compensation mechanism must occur in order to recover reasonable electrostatic valencies for all the oxygen ions.

2. *Increased Leach Resistance of $Ba_2Ti_9O_{20}$*

Inspection of Figs. 6a and 8 clearly shows that there are no continuous tunnels in this structure. The appearance of $[TiO_6]$ octahedra within the former hollandite tunnels will effectively prevent the relatively easy movement of Ba^{2+} or, for example, Cs^{137} along the "tunnels." Ba^{2+} ions are effectively locked, or at least blocked, within the structure. It is not clear yet whether the addition of ~5% Cs_2O replacing BaO significantly alters the framework structure, and further studies of Cs-exchanged specimens are in progress.

3. *Dielectric Response of Ba^{2+} in $Ba_2Ti_9O_{20}$*

The occurrence of the sequence of sites

O–Ba–□–Ba–O

along the [100] axis, with a vacant site between the two Ba^{2+}, allows space for Ba^{2+} ion hopping between filled and empty sites under the influence of an oscillatory electric field, at elevated temperatures. The geome-

try of this process is well defined and stable up to 1420°C, and Ba^{2+} ion movements are presumably much more localized (jumps of ± 2.9 Å only are allowed) than is the case for Ba^{2+} ions in hollandite or other partially occupied tunnel structures such as the alkali–titanate related structure of $BaTi_4O_9$ (*18*).

Acknowledgments

This work was financially supported by the Australian Research Grants Committee, the University of Melbourne, and by the SERC (U.K.). G. Grzinic is grateful for the award of a University of Melbourne Research Scholarship.

References

1. L. A. Bursill and G. Grzinic, *Acta Crystallogr. Sect. B* **36,** 2902 (1980).
2. W. Sinclair, G. M. McLaughlin, and A. E. Ringwood, *Acta Crystallogr. Sect. B* **36,** 2913 (1980).
3. A. E. Ringwood, S. E. Kesson, N. G. Ware, W. O. Hibberson, and A. Major, *Geochem. J.* **13,** 141 (1979).
4. H. M. O'Bryan, W. H. Grodkiewiez, and J. L. Bernstein, *J. Amer. Ceram. Soc.* **63,** 309 (1980).
5. G. Grzinic and L. A. Bursill, in preparation.
6. H. M. O'Bryan, J. Thomson, Jr., and J. K. Plourde, *J. Amer. Ceram. Soc.* **57,** 450 (1974).
7. J. P. Guha, *J. Solid State Chem.* **34,** 17 (1980).
8. Ekkhart Tillmanns, *Acta Crystallogr. Sect. B* **25,** 1444 (1969).
9. Ekkehart Tillmanns, *Cryst. Struct. Comm.* **1,** 1 (1972).
10. L. A. Bursill, A. E. C. Spargo, D. Wentworth, and G. J. Wood, *J. Appl. Cryst.* **12,** 279 (1979).
11. J. M. Cowley, "Diffraction Physics," North-Holland/American Elsevier, New York (1975).
12. D. J. Smith, R. A. Camps, V. E. Cosslett, L. A. Freeman, W. O. Saxton, W. C. Nixon, H. Ahmed, C. J. D. Catto, J. R. A. Cleaver, K. C. A. Smith, and A. E. Timbs, *Ultramicroscopy* **9,** 203 (1982).
13. G. Fallon and B. Gatehouse, private communication (1982).
14. G. Grzinic and L. A. Bursill, *Micron* **13,** 251 (1982).
15. L. A. Bursill and A. R. Wilson, *Acta Crystallogr. Sect. A* **33,** 672 (1977).
16. A. R. Wilson, Ph.D. Thesis, Univ. of Melbourne (1981).
17. L. A. Bursill, *Acta Crystallogr. Sect. B* **35,** 530 (1979).
18. K. Lukaszewicz, *Roczniki Chem.* 11, **31,** 1111 (1957).